JOURNAL OF SOLID STATE CHEMISTRY 37, 67–76 (1981)

A Thermochemical Study of the Phase Reaction $(1/7)Pr_7O_{12} + (1/7 - x/2)O_2 = PrO_{2-x}$

HIDEAKI INABA,* ALEXANDRA NAVROTSKY, AND LEROY EYRING

Department of Chemistry and Center for Solid State Science, Arizona State University, Tempe, Arizona 85281

Received December 20, 1979; in revised form June 9, 1980

The heat of reaction and equilibrium pressure for both the oxidation and reduction reactions, $(1/7)Pr_7O_{12} + (1/7 - x/2)O_2 = PrO_{2-x}$, have been measured by means of a Tian–Calvet-type calorimeter and thermal balance. The results of equilibrium pressure measurements under isothermal conditions show a reproducible and unsymmetrical hysteresis loop. The unsymmetrical hysteresis loop is interpreted as due to a different pattern of intergrowth formed during oxidation and reduction. The ordered intermediate phases (Pr_nO_{2n-2}) are intergrown coherently at the unit cell level with each other but not with the disordered α phase (PrO_{2-x}). The role of coherent intergrowth in both symmetric and unsymmetric hysteresis loops has been discussed. The partial molar enthalpy ($-\Delta\bar{H}_{O_2}$) is about 58 kcal/mole of O_2 in the Pr_7O_{12} phase; it increases slightly as O/Pr increases, then increases sharply to about 85 kcal/mole of O_2 around $PrO_{1.78}$. No difference in partial molar enthalpy is observed between the oxidation and reduction paths within the experimental error, even though different equilibrium pressures are observed depending upon the path. The slight increase in the partial molar enthalpy in the "two-phase" region is attributed to the interaction term of the different domains using the same regular solution model used to account for the hysteresis observed previously. The sharp change in $-\Delta\bar{H}_{O_2}$ around $PrO_{1.78}$ is believed associated with the phase change from the coherently intergrown ordered phases to the disordered α phase. The difference between the partial molar entropy on oxidation and that on reduction is explained by both the regular solution model and the usual thermodynamic treatment using the data of isothermal hysteresis.

1. Introduction

The higher praseodymium oxides belong to a fluorite-related homologous series. The intermediate phases of this series have narrow composition ranges and ordered structures (*1–4*) at low temperatures. At higher temperatures and higher oxygen pressures, a widely nonstoichiometric, disordered phase with fluorite structure (*5, 6*) becomes stable. The phase diagram of praseodymium oxide by Hyde *et al.* (*5*) is shown in Fig. 1. Thermodynamic studies of the phase transformation between these phases have shown that reproducible hysteresis loops are followed, when a phase reaction cycle is carried out between two phases (*5, 13*). Chemical hysteresis is far from being understood in spite of its frequent occurrence in phase transformations. In order to understand the nature and mechanism of this phenomenon it is necessary to have a detailed knowledge of the structural and thermodynamic relationships of the end mem-

* On leave from the Department of Nuclear Engineering, Faculty of Engineering, Nagoya University, Nagoya, Japan.

0022-4596/81/040067-10$02.00/0

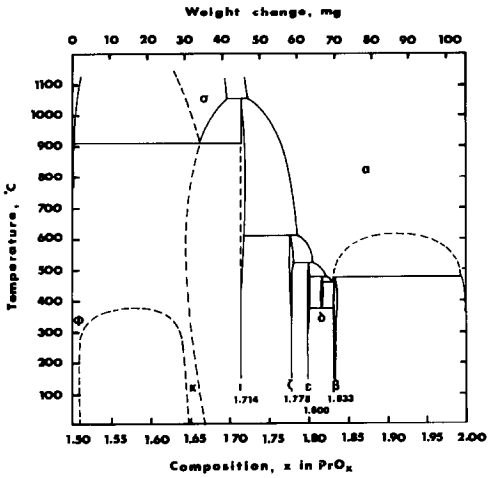

FIG. 1. Phase diagram of praseodymium oxide (see Ref. (5)).

bers of the phase reaction and the characteristics and kinetics of their intergrowth behavior. A thermodynamic model for the hysteresis loop has been proposed (*12*) in which the gross features of the main hysteresis loop are reproduced. A study of the relationship between thermodynamics and kinetics during hysteresis has been purused (*13*).

The direct observation of the heat of reaction at known pressures (compositions) provides the most important thermodynamic properties, $\Delta\bar{H}_{O_2}$, $\Delta\bar{G}_{O_2}$, and $\Delta\bar{S}_{O_2}$, respectively the partial molar enthalpy, Gibbs free energy, and entropy of oxygen in the oxide. This kind of measurement has been made in systems such as ZrO_x (*14*), MnO_{1+x} (*15*), UO_{2+x} (*16*), and CeO_{2-x} (*17*). Oxygen partial pressure measurements as a function of temperature together with compositional measurements have also provided values for $\Delta\bar{H}_{O_2}$, $\Delta\bar{G}_{O_2}$, and $\Delta\bar{S}_{O_2}$, in systems such as PuO_{2-x} (*18*), NbO_{2+x} (*19*), AmO_{2-x} (*20*), and CeO_{2-x} (*21*). In systems where reversible hysteresis exists, it is difficult to get accurate partial molar enthalpy values from the temperature dependence of pressure because the log P_{O_2} vs $1/T$ plot shows appreciable scatter of the data. In the present study, the direct heat of reaction along the hysteresis loop between the well-ordered ι and the disordered α phase has been measured and the derived $\Delta\bar{H}_{O_2}$ and $\Delta\bar{S}_{O_2}$ values have been interpreted using the thermodynamic model for hysteresis.

2. Experimental

2.1. Calorimeter

An isothermal twin microcalorimeter of the Tian–Calvet type used in these experiments (*22, 23*) has been described elsewhere. Some modifications of the specimen chamber were made to allow study of a solid–gas reaction. The quartz reaction tubes, with i.d. 19 mm and length 86 cm, are connected to a vacuum system through stopcocks and capillary tubes. The sample container is made of 20 platinum dishes 18.8 mm in diameter and 6 mm deep stacked within a platinum support. Oxygen gas is accessible to the oxide through 0.03-mm spaces between the dishes. The calorimetric sample is 13.8368 g of praseodynium oxide in the form of $PrO_{1.71400}$. A correction for the heat effect due to gas introduction is eliminated by introducing the gas simultaneously into both the sample and reference sides. The calorimeter is calibrated by dropping a piece of platinum into the sample chamber using a quartz tube of the same size. The enthalpy change for platinum between 713°C and room temperature is calculated using standard reference data, thus providing a calibration factor. The pressure was read by means of a Datametrics electronic manometer. The analog signal of the pressure was accurately digitized using a digital voltmeter.

The 99.9% pure oxygen was supplied by the Liquid Air Company and used without further purification. The praseodymium oxide was furnished by Research Chemical Division of Nucor Corporation as 99.999%

pure with respect to other rare earths. Typical percentages of impurities of other elements are Si,Fe < 0.01 and Mg,Ca < 0.005. This oxide was dissolved in 5 *N* HNO_3 and the solution neutralized to 1 *N* HNO_3 by the addition of NH_3 gas. The oxalate was precipitated using oxalic acid. The washed precipitate was decomposed to the oxide upon heating at 1000°C for 48 hr.

2.2. The Thermogravimetric Study

Thermodynamic measurements of praseodymium oxides (between the ι and α phases) also were carried out using an Ainsworth thermobalance, as described elsewhere (*13*). The same oxygen and oxide sample used in the calorimetric study was used. The sample consisted of 2.4285 g of $PrO_{1.714}$.

3. Results

3.1. The Heat Effect Due to Gas Introduction

The heat effect associated with the introduction of gas into the calorimeter has been studied by adding oxygen gas to or pumping it from one side of the calorimeter or admitting it to both sides simultaneously. Figure 2 shows the results. When 710 Torr of oxygen is introduced to one side, a significant exothermic effect of 1.49 cal and a baseline shift are observed. When it is evacuated an endothermic effect of 1.35 cal is observed. The heat effect due to gas introduction would be ΔnRT, where Δn is the effective number of moles of gas, R is the gas constant, and T is the absolute temperature. In the present case the effective volume is taken as 50 cm^3, ΔnRT = 1.13 cal. This is to be compared with the 1.49 or 1.35 cal observed. The larger values observed may be due to differences in heat transfer coefficient on the two sides, convection, or an error in estimating the effective volume. The agreement is considered satisfactory. After evacuation, 420 Torr of oxygen was introduced to both sides of the reaction tube simultaneously with only a negligibly small disturbance in the baseline (see Fig. 2). Therefore, the only correction to the observed enthalpy which needs to be made is that arising from the reacting oxygen.

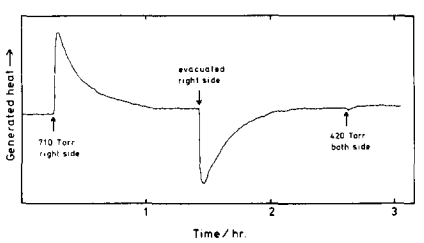

FIG. 2. The heat effect due to gas introduction or evacuation in the calorimeter (the integrated area corresponds to heat generated or released).

3.2. The Isothermal Hysteresis Loop for the Phase Transition ι to α

The composition of praseodymium oxide was measured as a function of pressure at 713°C by two different methods. One, obtained thermogravimetrically, is shown in Fig. 3a. The other, shown in Fig. 3b, was determined by measuring the pressure change when oxygen gas was absorbed in or released from the solid in the calorimeter. Agreement between the two different measurements is excellent. The shape of this hysteresis loop is not symmetrical, in contrast to the transition between the ι (Pr_7O_{12}) and ζ (Pr_9O_{16}) phases (*13*). This loop becomes markedly narrower as it approaches the α phase.

3.3. The Partial Molar Thermodynamic Quantities for the Transition between the ι and α Phases

Examples of the calorimetric measurements are given in Table I. After the system has reached equilibrium the oxygen pressure is increased suddenly to both sides of the reaction tube, and the compositional

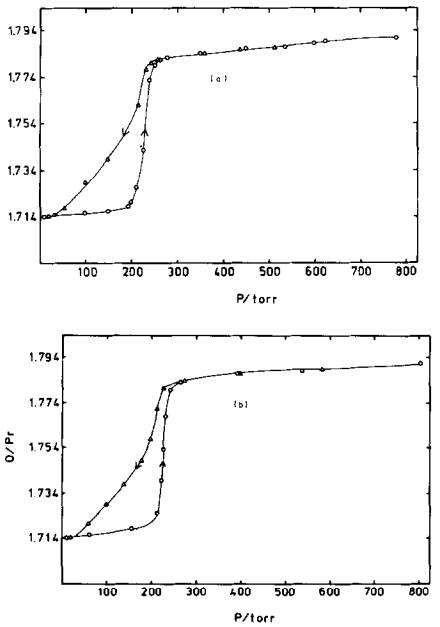

FIG. 3. Isothermal hysteresis loop between ι and α phases at 713°C by (a) weight measurement using Ainsworth thermal balance; (b) pressure measurement in the calorimeter. ○, Oxidation path; △, reduction path.

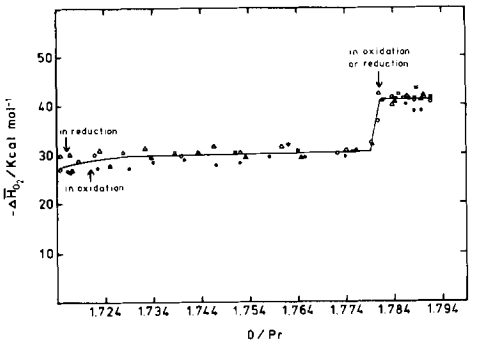

FIG. 4. The partial molar enthalpy as a function of composition. Two-phase regions are between arrows. B series: ○, oxidation; ●, reduction. C series: △, oxidation; ▲, reduction. E series: □, oxidation; ■, reduction.

change and heat generated are measured. According to Boureau and Kleppa (*24*), the partial molar enthalpy, $\Delta\bar{H}_{O_2}$, should be equal to $Q/\Delta n$ taking into account the work done by the gas; Q is the heat absorbed and Δn is the number of moles of gas absorbed by the solid. The reaction rate was fast in the one-phase region and a stable baseline was obtained within 70 min after the initiation of the reaction. In the two-phase region more than 2 hr was required to obtain a stable baseline. As seen in Fig. 4, within the experimental error, no difference in partial molar enthalpy is observed between the oxidation and reduction paths even though different equilibrium pressures are observed depending upon the path. The partial molar enthalpy throughout the two-phase region has a value similar to that of the ι phase. It then suddenly becomes higher as the α phase is formed. The partial

TABLE I

SOME EXAMPLES OF THE CALORIMETRIC RESULTS

Experiment number	Initial pressure (Torr)	Final pressure (Torr)	Compositional change Δx ($\times 10^{-3}$)	Average composition x in PrO_x	Absorbed heat (cal)	Partial molar enthalpy (kcal/mole of O_2)
CO-1	10.09	60.30	1.723	1.71486	−2.128	−30.05
CO-2	60.30	154.56	2.264	1.71686	−2.804	−30.13
CO-3	154.56	212.01	7.016	1.72292	−8.934	−30.98
CR-1	803.36	582.58	−2.640	1.79011	4.551	−41.94
CR-2	582.58	394.56	−3.329	1.78712	5.703	−41.68
CR-3	394.56	273.07	−3.189	1.78386	5.448	−41.57
CR-4	273.07	228.41	−1.867	1.78134	3.141	−40.93
CR-5	228.41	214.20	−9.004	1.77590	11.301	−30.54

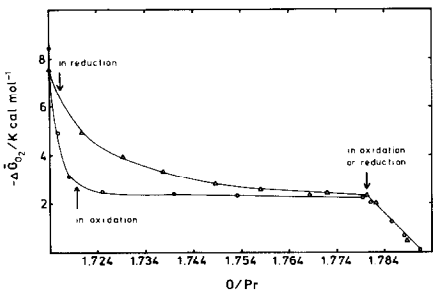

FIG. 5. The partial molar Gibbs free energy as a function of composition. O, Oxidation path; △, reduction path.

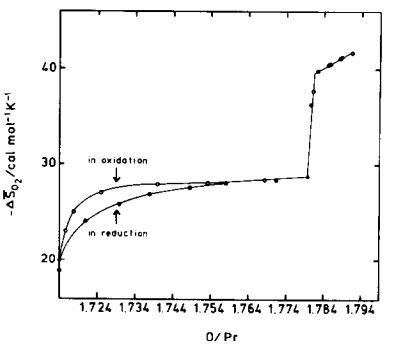

FIG. 6. The partial molar entropy as a function of composition. The two-phase regions are between arrows. O, Oxidation path; △, reduction path.

molar free energy $\Delta\bar{G}_{O_2}$ is obtained from the isothermal hysteresis curve shown in Fig. 3 using the relationship $\Delta\bar{G}_{O_2} = RT \ln P_{O_2}$. It is plotted against composition in Fig. 5. From $\Delta\bar{G}_{O_2}$ and $\Delta\bar{H}_{O_2}$, the partial molar entropy, $\Delta\bar{S}_{O_2}$, can be calculated, using the relationship

$$\Delta\bar{S}_{O_2} = \frac{\Delta\bar{H}_{O_2} - \Delta\bar{G}_{O_2}}{T}.$$

The results are plotted in Fig. 6, where the hysteretic effect is most apparent below a composition of $PrO_{1.75}$. There is a sharp change at the transition point between the region of single-phase α and the two-phase regions.

4. Discussion

4.1. Models

Point defect or clustered point defect models have been invoked to explain the partial molar thermodynamic quantities, $\Delta\bar{G}_{O_2}$ and $\Delta\bar{H}_{O_2}$, in systems such as MnO_{1+x} (*15*), VO_{2+x} (*25*), and NbO_{2+x} (*8*). The point defect model should not, however, be applied to compounds such as the rare earth oxides, R_nO_{2n-2}, having extended defects.

Recently Manes and Parteli (*26*) proposed a "tetrahedral defect" model for the thermodynamic quantities of fluorite-related compounds R_nO_{2n-2} and RO_{2-x}. They assume a complex of the tetrahedral defects in a spherical envelope of space as the extended defect. This model seems inappropriate for the fluorite-related rare earth oxides encountered here since the ordered intermediate phases are believed to consist of superstructures of $\{135\}_F$ planar arrays of paired oxygen vacancies along [111] across the metal atoms in the plane (*1–4*). The short-range order in the α phase has yet to be determined but it is believed to consist of local arrangements related to that of the ordered phases.

None of the existing statistical mechanical models appears to be applicable to the compounds R_nO_{2n-2} (n = 7–12) which have extended defects of the type described above. In a previous paper (*12*), a regular solution model was used to account for hysteretic behavior. It predicts the gross features of hysteresis but it cannot, for example, account for the fact that truly constant temperature regions are never observed in hysteresis loops associated with rare earth oxide systems. Furthermore, it gives a narrower compositional range of hysteresis than that observed when tabulated values of $\Delta H°$ and $\Delta S°$ are used. Nevertheless, we will apply this model to hysteresis in the partial molar thermodynamic quantities observed in this study.

Before applying the model to the experimental data of this study involving an order–disorder transition, let us examine the *isothermal* rather than the isobaric hysteretic behavior in the simpler system between the ι and ζ phases. This reaction can be represented in the following form:

$$MO_a + \tfrac{1}{2}bO_2 = MO_{a+b}. \quad (1)$$

When we let $MO_a = A$ and $MO_{a+b} = B$ the Gibbs free energy for the system would be

$$G = N_{O_2}\mu^\circ_{O_2} + N_A\mu^\circ_A + N_B\mu_B + (N_AN_B/N)\Gamma + NkT\{X_B \ln X_B + (1 - X_B) \ln (1 - X_B)\}, \quad (2)$$

where N_A and N_B are the numbers of A and B, respectively; μ°_A, μ°_B, and $\mu^\circ_{O_2}$ are the bulk chemical potentials of A, B, and oxygen gas, respectively; Γ is the net interaction energy between A and B; $N = N_A + N_B$; N_{O_2} is the number of moles of oxygen gas; and μ_{O_2} is the chemical potential of the oxygen gas ($\mu_{O_2} = kT \ln P_{O_2}$). G is minimized by holding the total of the metal atoms, N, and the oxygen atoms [$2N_{O_2} + aN_A + (a + b)N_B$] constant. The result is

$$\frac{b}{2}\mu_{O_2} = \frac{b}{2}kT \ln P_{O_2} = \mu_B - \mu_A + \Gamma(1 - 2X_B) + kT \ln \frac{X_B}{1 - X_B}. \quad (3)$$

There are three roots (X_B) of this equation if we choose the proper values for $\mu_B - \mu_A$ and Γ. Taking stable and metastable solutions (ignoring one unstable root), we get the hysteresis curve. When this equation is applied to the isothermal hysteresis curve between ι and ζ at 535°C (*11*) we have the results shown in Fig. 7, where the experimental curve is also given for comparison. (Here $b = 0.064$ and ($\mu_A - \mu_B$) and Γ are assumed to be $170k$ and $1676k$, respectively, as they are in the isobaric transition.) A constant pressure (chemical potential of oxygen gas) plateau is observed in the model similar to the constant-temperature region observed in the isobaric hysteresis (*12*) when plotted against composition, at variance with the experimental curve. A narrower compositional range of hysteresis is also observed in the model. In this calculation the entropy term in Eq. (2) is probably overestimated, because in the actual rare earth oxides, MO_a and MO_{a+b} do not act as elementary units. Rather m of these are associated as the elementary unit making the configurational entropy term of Eq. (2)

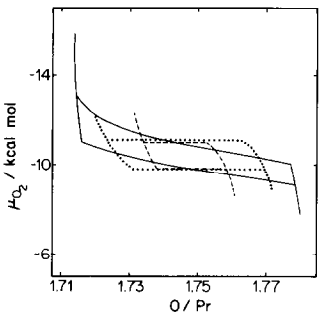

FIG. 7. Isothermal hysteresis loop between ι ($PrO_{1.714}$) and ζ ($PrO_{1.778}$) phases at 535°C. ——, Experimental data: – – –, model ($\Gamma = 1676k$, $\mu_A - \mu_B = 170k$ in Eq. (3)); · · · · ·, model ($\Gamma = 240k$, $\mu_A - \mu_B = 170k$ in Eq. (6)).

$$S = k \ln \frac{(N/m)!}{(N_A/m)!\,(N_B/m)!} \simeq -\frac{kN}{m}\{X_B \ln X_B + (1 - X_B) \ln (1 - X_B)\}. \quad (4)$$

G then becomes

$$G = N_{O_2}\mu_{O_2} + N_A\mu_A + N_B\mu_B + \frac{N_AN_B}{N}\Gamma + \frac{NkT}{m}\{X_B \ln X_B + (1 - X_B) \ln (1 - X_B)\}. \quad (5)$$

Minimizing G, we get

$$\frac{b}{2}\mu_{O_2} = \mu_B - \mu_A + \Gamma(1 - 2X_B) + \frac{kT}{m}\ln\frac{X_B}{1 - X_B}. \quad (6)$$

If we now assume that the unit cell is the elementary unit, m is 7 for the ι and 9 for the ζ phase. If we take m to be 8 as an average for both phases and solve Eq. (6), we get the hysteresis curve shown in Fig. 7, where $(\mu_A - \mu_B)$ and Γ are assumed to be $170k$ and $240k$, respectively. We can see from Fig. 7 that the compositional width of hysteresis approaches that observed but is still short. This means that we still overestimate the entropy term.

One of the many simplifying assumptions in the model is that the elementary unit size, m, is the same in both phases. Relaxing this assumption leads to the following results. If one uses m equal to 7 and 9 rather than the average, the effect in the calculation is to shift the hysteresis curve up slightly without changing its form. Indeed, any choice of parameters in the above model will result in a horizontal slope to the hysteresis loop (at variance with observation) (*12*). Work is under way on a domain model of hysteresis which will overcome this difficulty.

High-resolution electron microscopic studies (*27, 29*) on the rare earth oxides in the two-phase region reveal coherent intergrowth of the two phases as thin layers or microdomains only a few unit cells wide which seem to act as elementary units. In any case, the elementary unit is much larger than the unit cell and the entropy term has been overestimated. In order to estimate the entropy term properly, the domain theory of hysteresis must be developed.

4.2. Hysteresis and Partial Molar Thermodynamic Properties

As we have seen in the last section, the regular solution thermodynamic model gives a gross picture of hysteresis and we might also expect that it would give a qualitative interpretation for the partial molar thermodynamic quantities.

4.2.1. Isothermal hysteresis. As can be seen from Eqs. (5) and (6), the net interaction term Γ must be significant in order for hysteresis to occur. The increase of free energy due to this term is compensated for by an increase in the configurational entropy term. In order for the entropy term to be significant in the two-phase regions, the "domains" of the two phases should be disordered on a sufficiently small scale. From high-resolution transmission electron microscopy studies (*27, 29*) of the two-phase regions, a coherent intergrowth of thin layers of each phase is observed to be stacked in a disordered way. From these considerations, we may conclude that coherent intergrowth of two phases results in hysteresis.

The structures of the ι and ζ phases differ only in the b-axis length. Hence the structures are coherent in the a–c plane making intergrowth relatively simple and leading to a symmetrical hysteresis. In contrast, in the ι–α region (see Figs. 3 and 5) iosthermal hysteresis is not symmetrical, but is wider in the neighborhood of the ι phase than in that of the α phase. In the α phase, there is no long-range ordering of the oxygen vacancies, whereas in the ι phase there is ordering of the [111] oxygen vacancy pairs across metal atoms in $\{135\}_F$ planes. Thus, completely coherent intergrowth between the ι and α phases cannot occur and hysteresis would be expected to be minimized. Since hysteresis does occur, something else must be happening in the so-called "two-phase region."

The shapes of the hysteresis loop in Figs. 3a and b suggest the following interpretation. The oxidation branch is normal for the transition between two ordered phases such as ι and ζ as discussed above. This could result if, in fact, the ordered phases

of $n = 7$, 8, 9, and 10 were involved by coherent intergrowth in the reaction and the disordered α phase were formed when the composition reached about $PrO_{1.78}$. In the reduction branch, the shape of the curve suggests that as ordered phases appear, they are not intergrown with α and hysteresis is minimal. However, as α disappears and the ordered phases dominate, the specimen recovers its hysteretic behavior, but too late to preserve a symmetric form. This interpretation requires that the ordered intermediate phases be stabilized by intergrowth of a rather fine texture.

The high-temperature X-ray diffraction studies of this region show only the ι and α phases with sharp transitions between them (*6, 30*). This could be true if the texture of the intergrown ordered phases accommodated only very thin layers except for the final product, ι. An electron microscopic study (*27*) of "single-crystal" specimens produced under similar conditions confirms this interpretation if one assumes that the quenching procedure employed preserves the high-temperature state. That is, the ordered phases are always observed intergrown in the two-phase region whether in oxidation or reduction with no regions of a disordered phase seen until the composition reaches essentially the α region.

4.2.2. Partial molar enthalpy at constant temperature. Using the relation $\mu_A = \bar{H}_A - T\bar{S}_A$, etc., Eq. (5) can be rewritten as

$$\begin{aligned} G = {} & \bar{H}^\circ_{O_2} N_{O_2} \bar{H}^\circ_A N_A + \bar{H}^\circ_B N_B \\ & + \frac{N_A N_B}{N}\Gamma + \frac{NkT}{\alpha}\{X_B \ln X_B \\ & + (1 - X_B)\ln(1 - X_B)\} \\ & - T\bar{S}_{O_2} N_{O_2} - T\bar{S}_A N_A - T\bar{S}_B N_B. \end{aligned} \quad (7)$$

Dividing by N and abstracting the enthalpy part (H) of Eq. (7), we get

$$\begin{aligned} H = {} & \bar{H}^\circ_A (1 - X_B) + \bar{H}^\circ_B X_B \\ & + X_B (1 - X_B)\Gamma + \frac{N_{O_2}}{N}\bar{H}^\circ_{O_2}, \end{aligned} \quad (8)$$

where $\bar{H}^\circ_{O_2}$ is the partial molar enthalphy of oxygen.

$$\bar{H}_{O_2} = \frac{\mu R 2/T}{\partial(1/T)} = k\frac{\partial(\ln P_{O_2})}{\partial(1/T)}. \quad (9)$$

Taking the derivative of Eq. (8) in order to get the partial molar quantity, we have

$$\begin{aligned} & \frac{b}{2}\Delta\bar{H}^\circ_{O_2} \\ & = \frac{dH}{dX_B} = -\bar{H}^\circ_A + \bar{H}^\circ_B + (1 - 2X_B)\Gamma \\ & - \frac{b}{2}k\frac{\partial(\ln P_{O_2})}{\partial(1/T)} + \frac{N_{O_2}}{N}\frac{\partial^2(\ln P_{O_2})}{\partial(1/T)\partial X_B}, \end{aligned} \quad (10)$$

assuming Γ is independent of X_B.

Only the last two terms of Eq. (10) depend on the path of the reaction and, hence, could account for hysteresis. Although the difference between the oxidation and reduction paths is smaller than the calculated standard deviation, Fig. 4 appears to show a systematic difference between points taken during oxidation and reduction. This is consistent with a small hysteresis in $\Delta\bar{H}$. Equation (10) also suggests that if the interaction term Γ is sufficiently small, the partial molar enthalpy would be constant in the two-phase region. In the usual case, such as α-Zr + ZrO_{2-y} (*14*), NbO + NbO_2 (*18*), and NbO_2 + $NbO_{2.42}$ (*18*), partial molar enthalpy is independent of composition. However, in the present case, Γ is not negligibly small and a slight increase in $-\Delta\bar{H}_{O_2}$ occurs as O/Pr increases, as shown in Fig. 4. When Γ is taken to be $240k$, as was assumed on the basis of the unit cell as an elementary unit in Section 4.1, the slope is too steep when compared with the experimental data. If an elementary unit larger than the unit cell were assumed, a small Γ would fit the experimental data. Actually, however, the interpretation is not as simple as represented in Eq. (10) because the net interaction term Γ may decrease as O/Pr in-

creases due to a reduction in the coherent intergrowth.

The sharp change in $-\Delta\bar{H}_{O_2}$ around $PrO_{1.78}$ accompanies the phase change from the coherently intergrown ordered phases to the disordered α phase. The magnitude of $-\Delta\bar{H}_{O_2}$ in the α region can be compared with previous data (*28*), ranging from 45 to 65 kcal/mole of O_2 in a generally higher composition range. The sharp break downward suggested by the curves of Jenkins *et al.* at about $PrO_{1.85}$ is confirmed by these results. That the values are more negative for the α phase than for the ι phase suggests that tighter bonding exists in the α phase as might be expected from the fact that the lattice parameter of the α phase is smaller than the pseudocubic parameters of the ι phase (*6*).

It is not clear why $-\Delta\bar{H}_{O_2}$ to form a higher oxidation state in the nonstoichiometric ι region is close to that to form a higher oxidized ordered phase. Part of the reason may be that $-\Delta\bar{H}_{O_2}$ in the "two-phase region" is decreased by the interaction term due to coherent intergrowth.

4.2.3. Partial molar entropy. We can get the entropy term (S) of the system from Eq. (*7*):

$$S = -\frac{k}{m}\{X_B \ln X_B + (1 - X_B)\ln(1 - X_B)\} + \bar{S}_A(1 - X_B) + \bar{S}_B X_B - \frac{N_{O_2}}{N} k \ln P_{O_2}. \quad (11)$$

Taking the derivative of Eq. (11), we get the partial molar entropy

$$\frac{b}{2}\Delta\bar{S}_{O_2} = \frac{dS}{dX_B} = \frac{k}{m}\ln\frac{1 - X_B}{X_B} - \bar{S}_A + \bar{S}_B + \tfrac{1}{2}bk \ln P_{O_2}. \quad (12)$$

Information about hysteresis in $\Delta\bar{S}_{O_2}$ is included in the final term of Eq. (12) since the other three terms on the right side do not depend on the path of the reaction. The difference between the entropy change per mole of O_2 in oxidation, S_1, and that in reduction, S_2, at the same composition is, from Eq. (12),

$$\Delta S = S_2 - S_1 = R \ln P_1/P_2, \quad (13)$$

where P_1 and P_2 are the equilibrium O_2 pressures in the oxidation and reduction paths, respectively. Equation (13) can also be obtained from the following argument:

$$\Delta S = S_2 - S_1 = -\frac{\partial(\bar{G}_{O_2,2} - \bar{G}_{O_2,1})}{\partial T} = -\frac{\partial(RT \ln P_2/P_1)}{\partial T} = -R \ln P_2/P_1 - RT\frac{\delta \ln P_2/P_1}{\partial T} \quad (14)$$

If the shape of the hysteresis curve does not depend on the temperature as is the case between ι and ζ phases (*11*), $\partial(\ln P_2/P_1)/\partial T = 0$, making Eq. (14) the same as Eq. (13). ΔS is calculated at the same composition using Eq. (13) and the hysteresis data from Fig. 3 and is plotted in Fig. 8, where ΔS, calculated from Fig. 6, is also shown for comparison. The agreement between them is very good.

The shape of the curve when $-\Delta\bar{S}_{O_2}$ is plotted against composition fits Eq. (11)

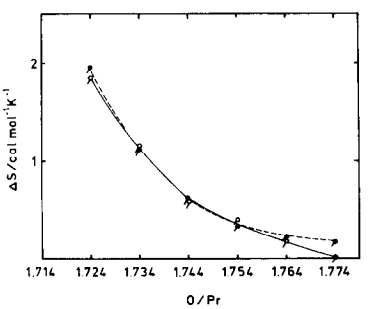

FIG. 8. A comparison of the partial molar entropy change at constant composition between that observed in oxidation and reduction (Fig. 6), ○, and that calculated using Eq. (13), ●.

well around the composition $X_B = 0.5$, but it does not fit well as $X_B \to 0$ or 1, which may be due to the oversimplification of the model. The observed sharp change in $-\Delta\bar{S}_{O_2}$ around $PrO_{1.78}$ accompanies the order–disorder phase transformation.

From the above data, one can conclude the following. The calorimetric and thermobalance measurements give consistent values of composition as a function of pressure. The gross features of the variation of $\Delta\bar{H}_{O_2}$ and $\Delta\bar{S}_{O_2}$ with composition can be explained by the regular solution model.

The detailed thermochemical data can be the basis of development of a more sophisticated theory.

Acknowledgment

This work has been supported by the National Science Foundation through Grants DMR 78-05722 and DMR 78-10038.

References

1. P. KUNZMANN AND L. EYRING, *J. Solid State Chem.* **14**, 229 (1975).
2. A. J. SKARNULIS, E. SUMMERVILLE, AND L. EYRING, *J. Solid State Chem.* **23**, 59 (1978).
3. E. SUMMERVILLE, R. T. TUENGE, AND L. EYRING, *J. Solid State Chem.* **24**, 21 (1978).
4. R. T. TUENGE AND L. EYRING, *J. Solid State Chem.* **29**, 165 (1979).
5. B. G. HYDE, D. J. M. BEVAN, AND L. EYRING, *Philos. Trans. Roy. Soc. London Ser A* **259**, 583 (1966).
6. D. A. BURNHAM AND L. EYRING, *J. Phys. Chem.* **72**, 4415 (1968).
7. D. A. BURNHAM, L. EYRING, AND J. KORDIS, *J. Phys. Chem.* **72**, 4424 (1968).
8. J. KORDIS AND L. EYRING, *J. Phys. Chem.* **72**, 2044 (1968).
9. R. P. TURCOTTE, M. S. JENKINS, AND L. EYRING, *J. Solid State Chem.* **7**, 454 (1973).
10. A. T. LOWE AND L. EYRING, *J. Solid State Chem.* **14**, 383 (1975).
11. A. T. LOWE, K. H. LAU, AND L. EYRING, *J. Solid State Chem.* **15**, 9 (1975).
12. D. R. KNITTEL, S. P. PACK, S. H. LIN, AND L. EYRING, *J. Chem. Phys.* **67**, 134 (1977).
13. H. INABA, S. PACK, S. H. LIN, AND L. EYRING, *J. Solid State Chem.* **33**, 295 (1980).
14. G. BOUREAU AND P. GERDANIAN, *High Temp. High Press.* **2**, 681 (1970).
15. C. PICARD AND P. GERDANIAN, *J. Solid State Chem.* **11**, 190 (1974).
16. P. GERDANIAN AND M. DODE, "Thermodynamics of Nuclear Materials," p. 41, Intern. At. Energy Agency, Vienna (1968).
17. J. CAMPSERVEUX AND P. GERDANIAN, *J. Chem. Thermodyn.* **6**, 795 (1974).
18. M. H. RAND, "Atomic Energy Review," Vol. 4, Special Issue No. 1, Intern. At. Energy Agency, Vienna (1966).
19. J. F. MARUCCO, R. TETOT, P. GERDANIAN, AND C. PICARD, *J. Solid State Chem.* **18**, 97 (1976).
20. T. D. CHIKALLA AND L. EYRING, *J. Inorg. Nucl. Chem.* **29**, 2281 (1967).
21. D. J. M. BEVAN AND J. KORDIS, *J. Inorg. Nucl. Chem.* **26**, 1509 (1964).
22. A. NAVROTSKY, *Phys. Chem. Minerals* **2**, 89 (1977).
23. A. NAVROTSKY, *Earth Planet. Sci. Lett.* **19**, 471 (1973).
24. G. BOUREAU AND O. J. KLEPPA, *J. Chem. Thermodyn.* **9**(6), 543 (1977).
25. P. GERDANIAN, *J. Phys. Chem. Solids* **35**, 163 (1974).
26. L. MANES AND E. PARTELI, private communication.
27. K. FORGHANY, H. INABA, AND L. EYRING, unpublished work.
28. M. S. JENKINS, R. P. TURCOTTE, AND L. EYRING, "The Chemistry of Extended Defects in Non-Metallic Solids" (L. Eyring and M. O'Keeffe, Eds.), North-Holland, Amsterdam (1970).
29. L. EYRING AND R. T. TUENGE, *J. Solid State Chem.* **29**, 165 (1979).
30. L. EYRING, unpublished work.